Supporting Information

Effect of Molecular Structures of Donor Monomers of Polymers on Photovoltaic Properties

Ruiping Qin,[*,†,‡] Deen Guo,[‡] Heng Ma,[‡] Jien Yang,[†,‡] Yurong Jiang,[‡] Hairui Liu,[†,‡] Zhiyong Liu,[‡] Jian Song[§] and ChaoChao Qin [*,§]

[†] Key Laboratory of Photovoltaic Materials of Henan Province, School of Material Science and Engineering, Henan Normal University, Xinxiang 453007, China.

[‡] Key Laboratory of Photovoltaic Materials of Henan Province, School of Physics, Henan Normal University, Xinxiang 453007, China.

[§] School of Physics, Henan Normal University, Xinxiang 453007, China.

Correspondence to: E-mail: Ruiping Qin (qinruiping@163.com)

EXPERIMENTAL

Materials and Instruments

Chemicals were purchased from commercial suppliers and used without further purification. THF/toluene were distilled from sodium with benzophenone as an indicator under nitrogen atmosphere. Chloroform were distilled from CaH_2. All the polymers chemical structure was diagrammed in Scheme 1. HXS-1; HXS-4(5) were prepared according to literature procedures. [1-2] Details of the synthesis of HXS-2(3) and the necessary intermediates are described in follow. (Schemes S1; S2 and Figures. S9-15) All reactions were performed under an atmosphere of nitrogen and monitored by thin layer chromatography (TLC) on silica gel 60 F254 (Merck, 0.2 mm). Column chromatography was carried out on silica gel (200-300 mesh). ^{1}H and ^{13}C NMR spectra were recorded on a Bruker AV 400 spectrometer

in $CDCl_3$. Electronic absorption spectra were obtained on a SHIMADZU UV-vis NIR UV-3600. GPC measurements were performed on Waters 410 system calibrated with polystyrene standards with Chloroform as eluent. The electrochemical behaviors were investigated by cyclic voltammeter (IviumStat A25361) using a standard three-electrode electro-chemical cell, in a 0.1 M tetrabutylammonium hexafluoro phosphate solution in CH_3CN, at room temperature and at N_2 atmosphere with a scanning rate of 0.05 V/S. An Au working electrode, a Pt wire counter electrode, and an $Ag/AgNO_3$ (0.01M in CH_3CN) reference electrode were used. The experiments were calibrated with the standard ferrocene/ ferrocenium (Fc) redox system, assuming that the energy level of Fc is 4.8 eV below vacuum.

Fabrication and Characterization of PSCs

OSCs were fabricated with the device configuration of ITO/ ZnO /polymer: $PC_{71}BM$ (1:2.5 weight ratio, 2.5%V, 1,8-diiodooctane) Blend/ MoOx/Ag. The conductivity of ITO was 15 Ω/□. A thin layer of the sol–gel ZnO was spin coated on top of cleaned ITO substrate at 3500 rpm/s and dried subsequently at 200 °C for 20 min on a hotplate before transferred into a glove box (Braun MB200MOD). The active layer was prepared by spin-coating the dichlorobenzene solution of polymers and $PC_{71}BM$ (with a 7 mg mL^{-1} concentration) on the top of ITO/ ZnO at 1500 rpm/s for 1 minutes. The top electrode was thermally evaporated, with a 0.8 nm MoOx layer, followed by 100 nm of Ag at a pressure of 10^{-7} Torr through a shadow mask. Six cells were fabricated on one substrate and the effective area of one cell is 4 mm^2. Atomic force microscopy (AFM) measurements were performed under ambient conditions using a Digital Instrument Multimode Nanoscope IIIA operating in the tapping mode. Transmission electron microscopy (TEM) images were obtained with a FEI Technai TF20 (Philip) transmission electron microscopy. The crystal structure was evaluated by X-ray diffraction (XRD) with Cu Ka radiation (Bruker AXS D8 Advance XRD system, k = 0.1542 nm). Solar cell characterizations were performed using a Keithley 2400 source meter and a solar simulator (Newport 91191) with an AM 1.5 filter. The external quantum efficiency (EQE) spectra were measured using a spectral response system (QTest Station 1000ADI, CROWNTECH) in a spectral range of 300–1100 nm.

Charge Mobility

the hole and electron mobility were determined by using the space charge limited current (SCLC) method. Device structures are ITO/PEDOT:PSS/ polymer:$PC_{71}BM$ /Au for hole-only devices and ITO/ZnO/ Polymer:$PC_{71}BM$ /Al for electron-only devices. The SCLC mobilities were calculated by

using the Mott–Gurney equation:

$$J = \frac{9\varepsilon_r \varepsilon_0 \mu V^2}{8L^2}$$

where J is the current density, ε_r is the relative dielectric constant of the active layer material usually 2–4 for organic semiconductors, herein we use a relative dielectric constant of 3, ε_0 is the permittivity of empty space, μ is the mobility of holes or electrons, L is the thickness of the active layer and V is the internal voltage of the device, and $V = V_{app} - V_{bi}$, where Vapp is the voltage applied to the device and V_{bi} is the built-in voltage resulting from the relative work function difference between the two electrodes.

Transient Absorption Spectroscopy.

Transient absorption (TA) spectra were measured in the preliminary experiment, we dissolved polymers in the solution of chlorobenzene with a concentration of 2 mg/250 mL at 25 °C to yield a maximum visible optical density between 0.2 and 0.4 in cuvettes with a 10-mm path length. The femtosecond transient absorption (fs-TA) spectrum were measured in the combined utilization of the Femtosecond Laser System (Coherent) and the Helios Pump-Probe System (Ultrafast Systems LLC), which was a commonly utilized time-resolving method and was considered to be one of the most effective tool for detecting the dynamics information in electronic excited state. The 450 nm pump pulses were generated from optical parametric amplifier (TOPAS-800-fs), which was pumped by the 800 nm fundamental beam out put from Femtosecond Laser System. The white light continuum probe beam (in the range from 400 to 1,500 nm) was generated by focusing a small portion (~10 μJ) of the regenerative amplifier's fundamental 800 nm laser pulses into either a 2 mm sapphire crystal (for visible range) or a 1 cm sapphire crystal (for NIR range). The pump and probe beams intersect on the sample at a particular angle. In order to achieve high signal-to-noise ratios, 5 to 10 scans of the data were collected in the measurement and the signal amplitude in the fs-TA measurements were averaged for further analysis.

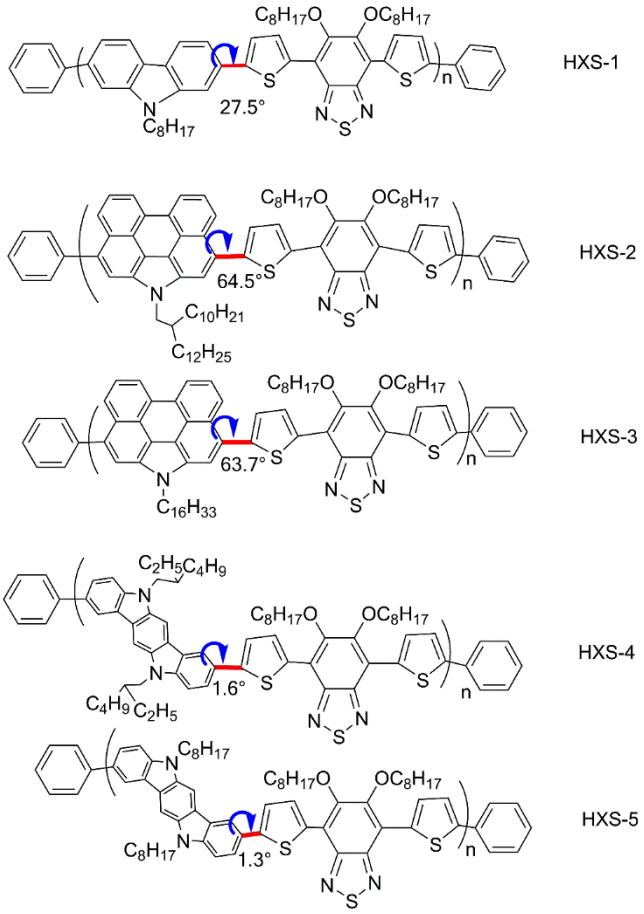

Figure S1. The torsion angle between carbazole architecture and acceptor blocks. For the torsion angle between different planar blocks, a computer simulation was carried out for these molecules. In our calculation, the energy-minimization and structural-optimization have been determined using a semiempirical molecular orbital package (MOPAC2000) with the key words AM1 and POLAR.

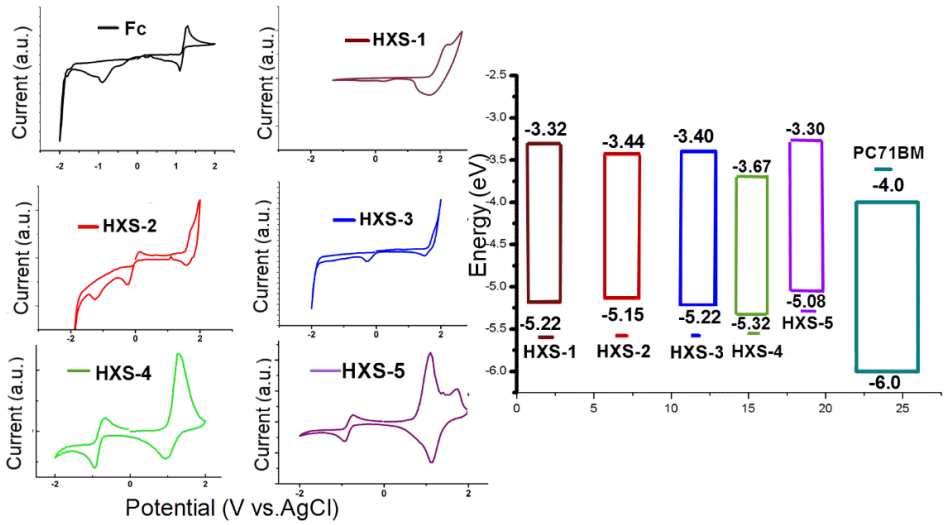

Figure S2. Cyclic voltammogram of copolymers and experimental energy levels.

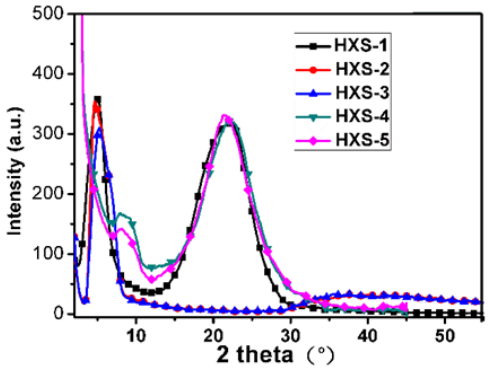

Figure S3. XRD diffraction pattern of the polymers sample powder.

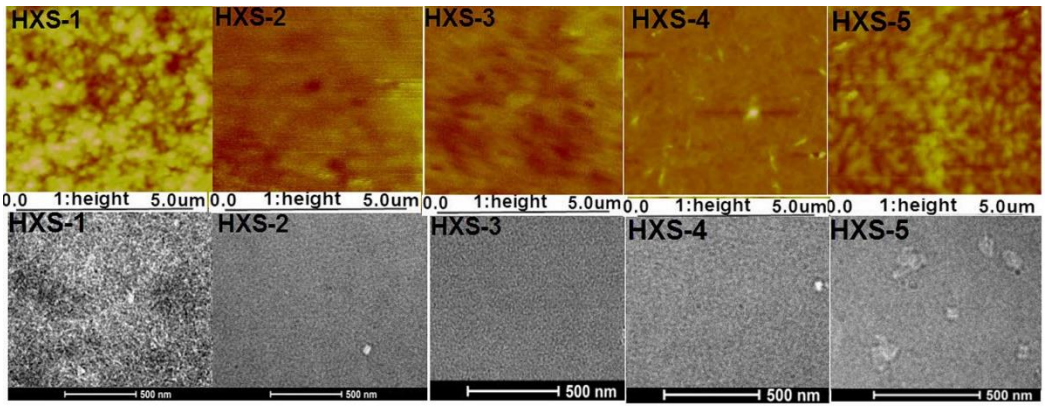

Figure S4. Height images by AFM and TEM of blend films.

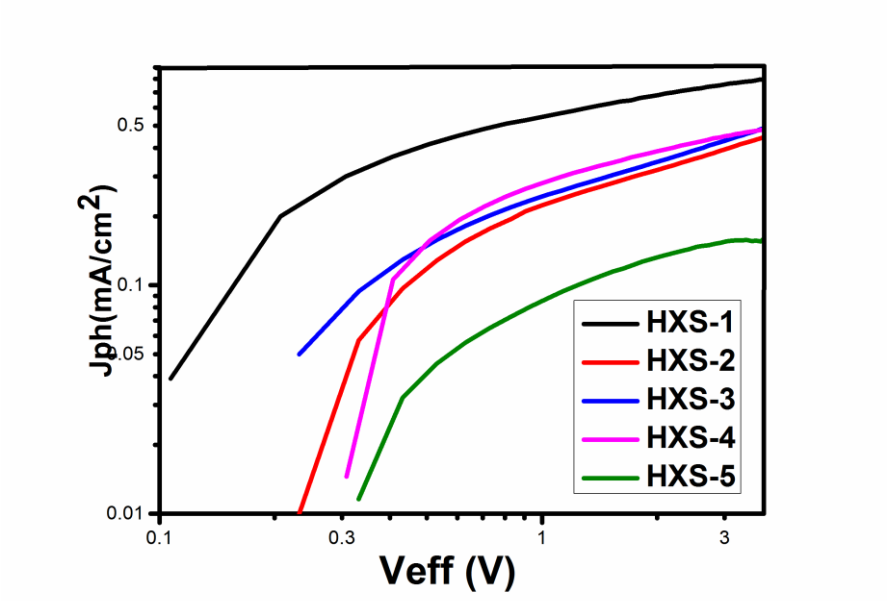

Figure S5. Photocurrent (Jph) versus effective voltage (Veff) curves. J_{ph} is defined as $J_{ph} = J_L - J_D$, where J_L and J_D are the photocurrent densities under illumination and in the dark, respectively. V_{eff} is defned as $V_{eff} = V_0 - V_a$, where V_0 is the voltage where J_{ph} equals zero and V_a is the applied bias voltage. $P_{diss} = Jph/Jph_{sat}$.

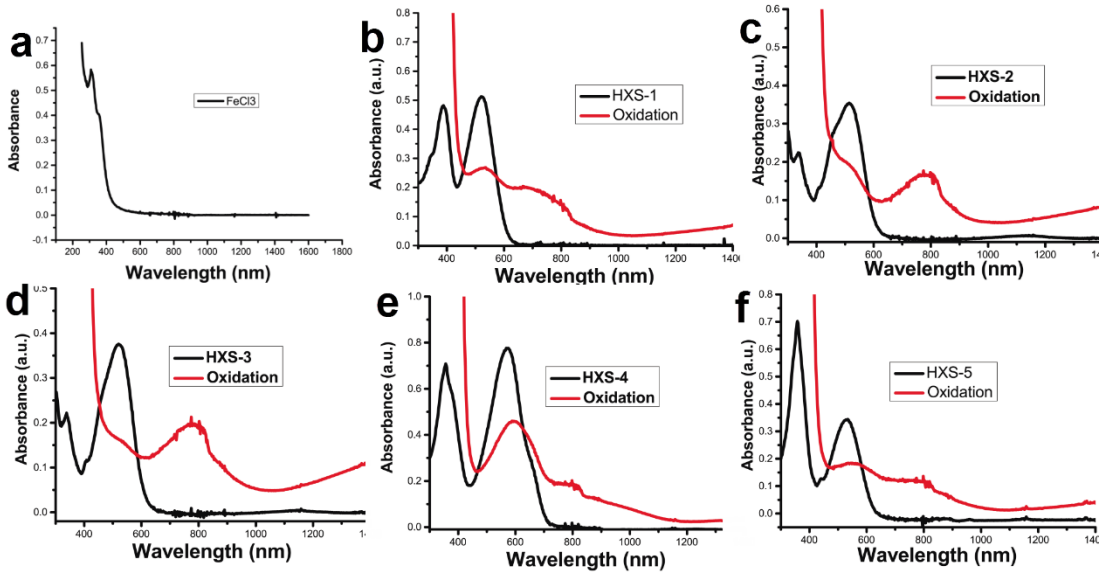

Figure S6. a) $FeCl_3$ absorption spectrum in chloroform. b, c, d, e, f) is steady-state absorption spectra for all polymers before (black) and after (red) addition of $FeCl_3$.

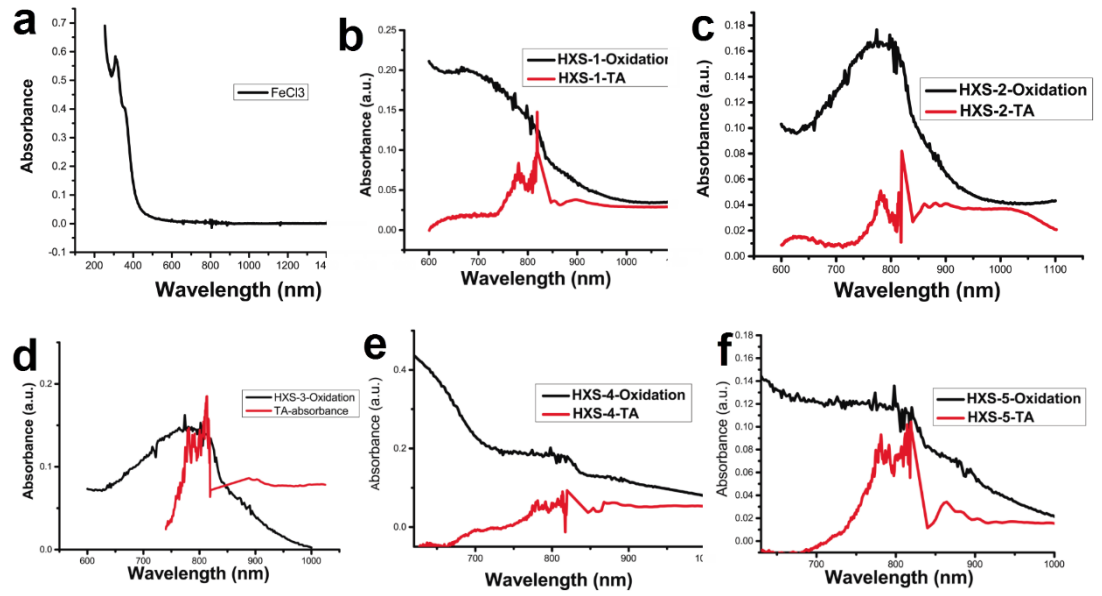

Figure S7. a) $FeCl_3$ absorption spectrum in chloroform. b, c, d, e, f) is corresponding to all polymers oxidation with $FeCl_3$ and their transient absorption spectrum at 1ps (before 819nm and after 846 nm was tested by different detectors).

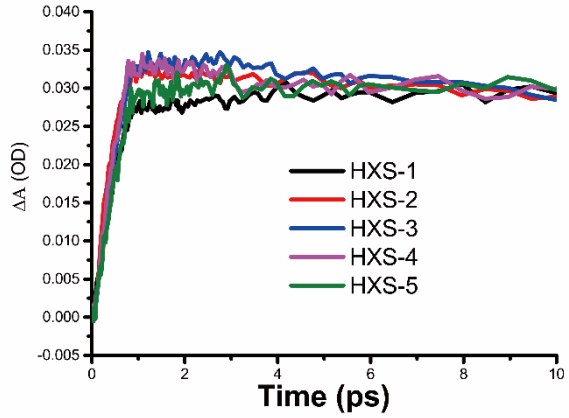

Figure S8. Kinetic traces for all polymers transient spectroscopic features detected at 1200 nm.

Table S1 the life time for different species of polymers[a]

Polymer	CS (τ_1) ns	ICSS (τ_2) ns
HXS-1	2.62	2.60
HXS-2	6.76	1.22
HXS-3	6.83	1.07
HXS-4	1.85	1.72
HXS-5	2.73	1.69

a. calculated based on kinetic traces for all polymers at 900 nm (τ1); 1200 nm (τ2).

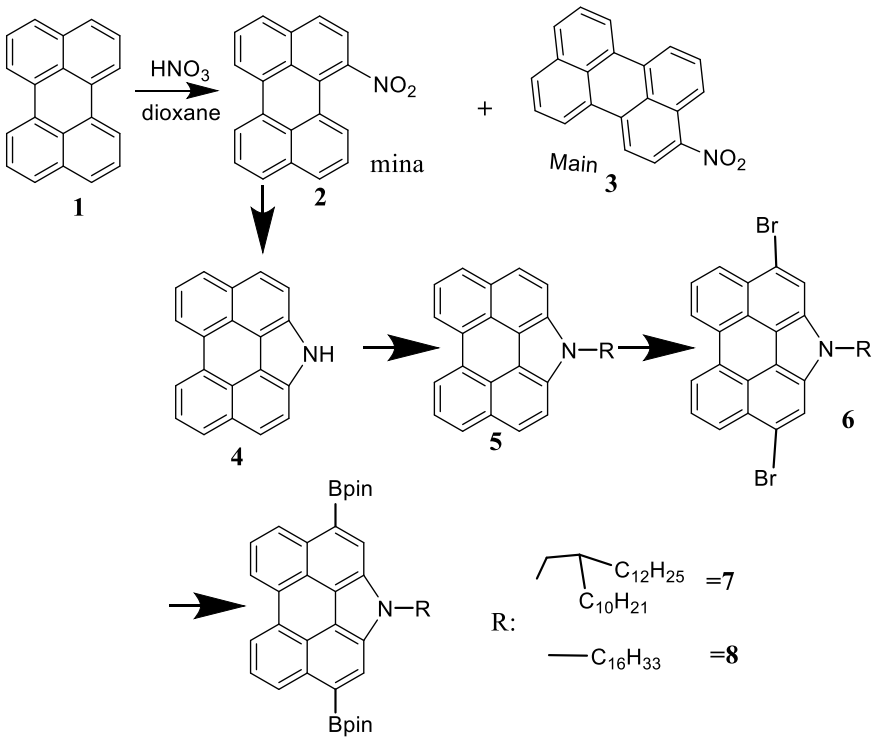

Scheme S1. The synthesis route towards intermediate **7** and **8**.

Compound **7**, **8** were synthesized similar according to the literature [3-6] and the synthesis route showed in Scheme 1 above.

The synthesis procedure of **HXS-2** and **HXS-3** is similar to **HXS-1** (see our previous work)[2]. **HXS-2**: **7** (0.2 g, 0.29 mmol), **8** (0.2 g, 0.29 mmol), $NaHCO_3$ (0.6 g, 7.14 mmol), H_2O 3 mL, THF 60 mL, $Pd(PPh_3)_4$ (6 mg). 212 mg (yield 69%) of black powder was obtained. ^1H NMR (500 MHz, $CDCl_3$) δ 8.78-7.08 (m, 12H), 4.65-4.19 (m, 6H), 2.39-2.06 (m, 5H), 1.56-1.12 (m, 73H), 0.89-0.80 (m, 12H).

^{13}C NMR (126 MHz, $CDCl_3$) δ 151.55, 150.52, 145.44, 145.35, 132.77, 131.48, 127.88, 127.07, 125.05, 123.75, 121.31, 117.52, 114.40, 74.81, 50.10, 39.93, 31.91, 30.59, 26.15, 22.67, 14.11. Element Analysis for $[C_{82}H_{113}N_3O_2S_3]n$: Calcd.: C, 77.61; H, 8.98; N, 3.31; O, 2.52; S, 7.58, Found: C, 76.66; H, 9.45; N, 2.53. Number Average Molecular Weight (Mn), 22.37 kg/mol; Weight Average Molecular Weight (Mw), 43.29 kg/mol; Polydispersity Index (PDI), 1.93.

HXS-3: **7** (0.26 g, 0.35 mmol), **8** (0.33 g, 0.35 mmol), $NaHCO_3$ (0.6 g, 7.14 mmol), H_2O 5 mL, THF 80 mL, $Pd(PPh_3)_4$ (10 mg). 253 mg (yield 51%) of black powder was obtained. ^1H NMR (500 MHz, $CDCl_3$) δ 8.77-7.66 (m, 12H), 4.76-4.32 (m, 6H), 2.18-2.11 (m, 6H), 1.57-1.17 (m, 6H), 0.86 (m, 9H). ^{13}C NMR (126 MHz, $CDCl_3$) δ 151.85, 151.12, 134.19, 132.13, 131.48, 130.67, 129.75, 127.78, 127.13, 125.04, 124.89, 121.24, 117.53, 114.76, 74.62, 37.35, 31.93, 31.33, 30.61, 29.72, 29.38, 27.30, 26.17, 22.70. Element Analysis for $[C_{82}H_{113}N_3O_2S_3]n$: Calcd.: C, 77.61; H, 8.98; N, 3.31; O, 2.52; S, 7.58 Found: C, 76.40; H, 8.74; N, 3.01. (Mn), 26.76 kg/mol; (Mw), 46.62 kg/mol; (PDI), 1.74.

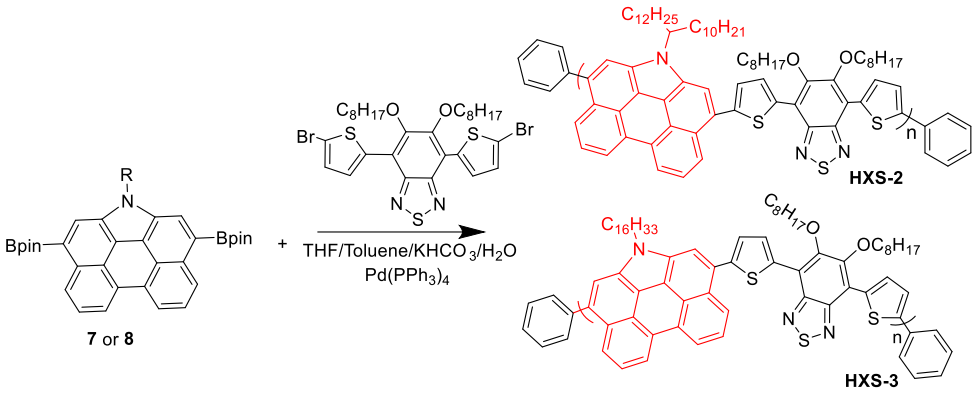

Scheme S2. Synthetic Routes of copolymers HXS-2 and HXS-3.

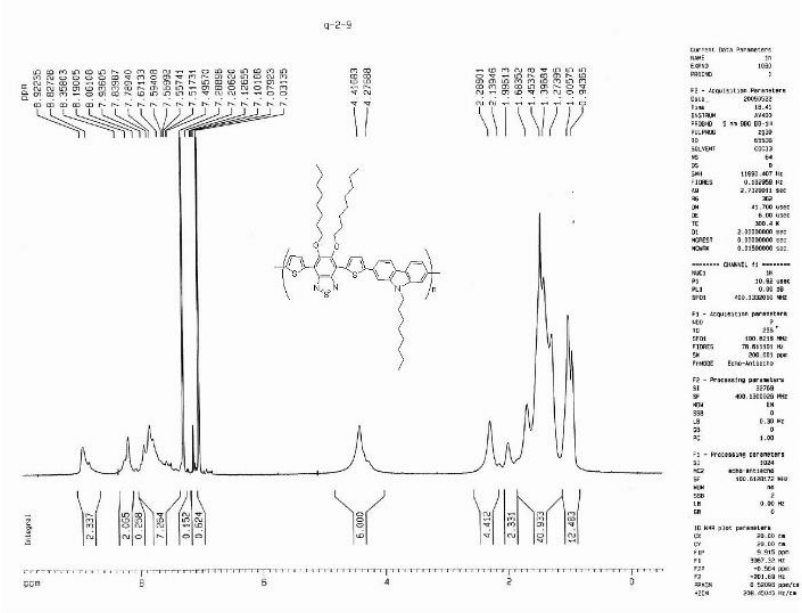

Figure S9. The ^{1}H NMR spectra of HXS-1.

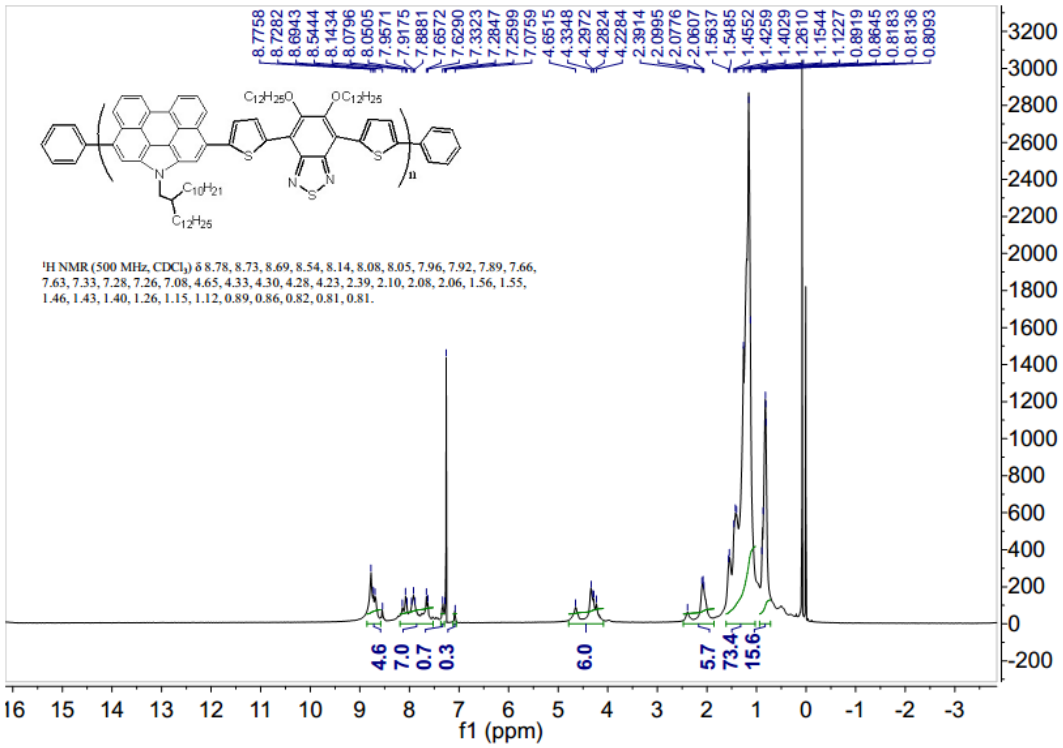

Figure S10. The ^{1}H NMR spectra of HXS-2.

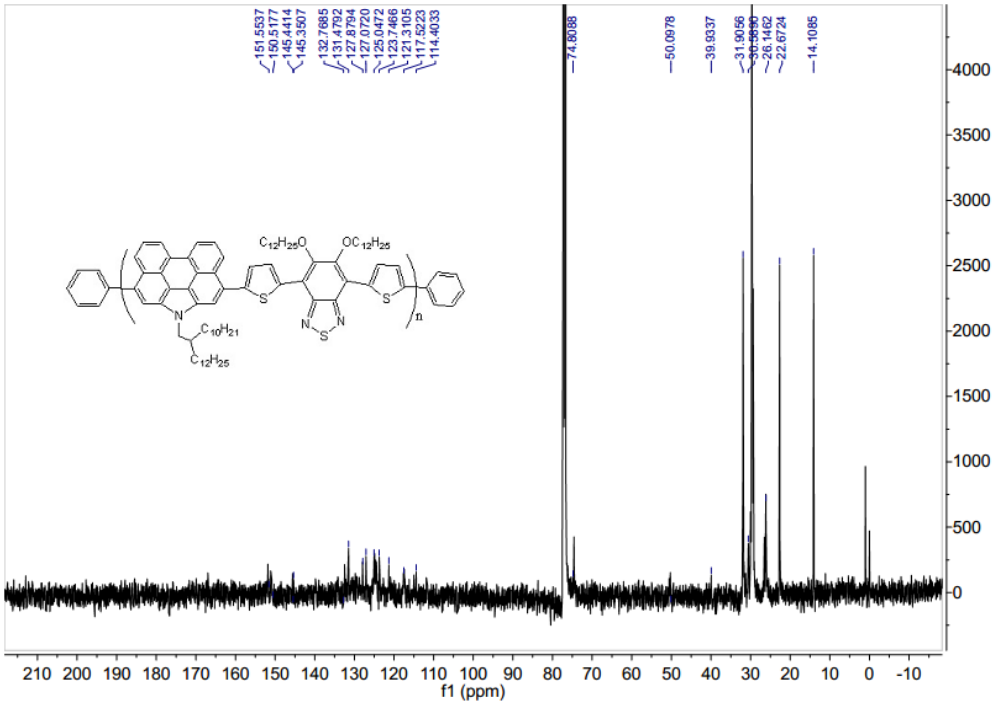

Figure S11. The ^{13}C NMR spectra of HXS-2.

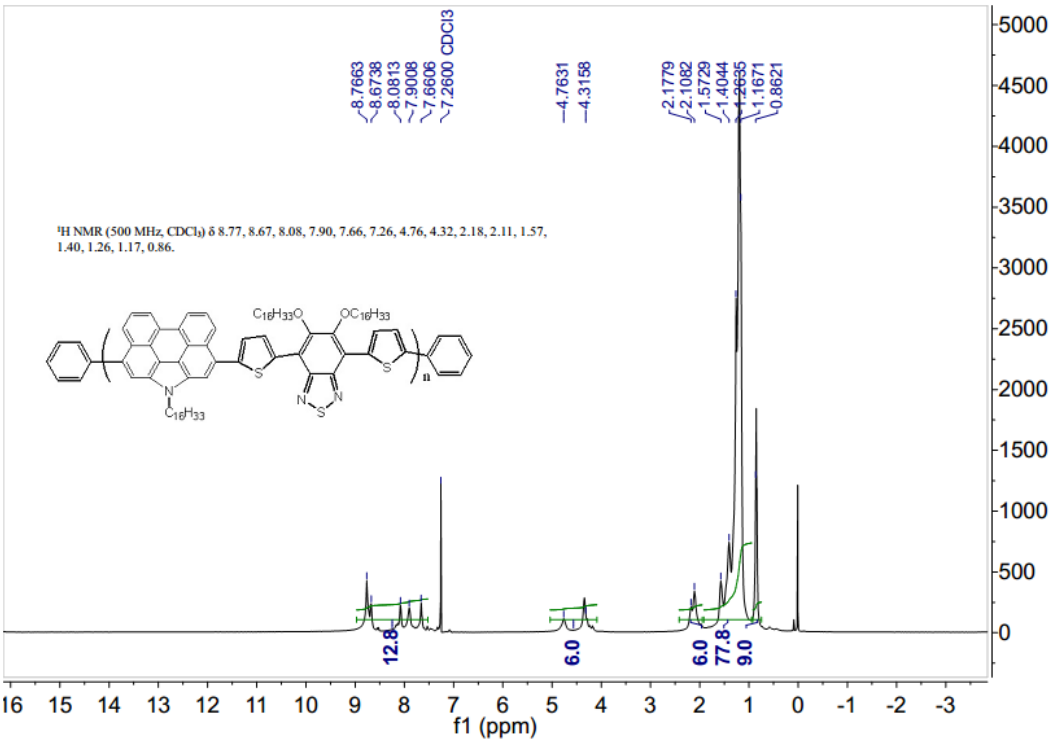

Figure S12. The ^{1}H NMR spectra of HXS-3.

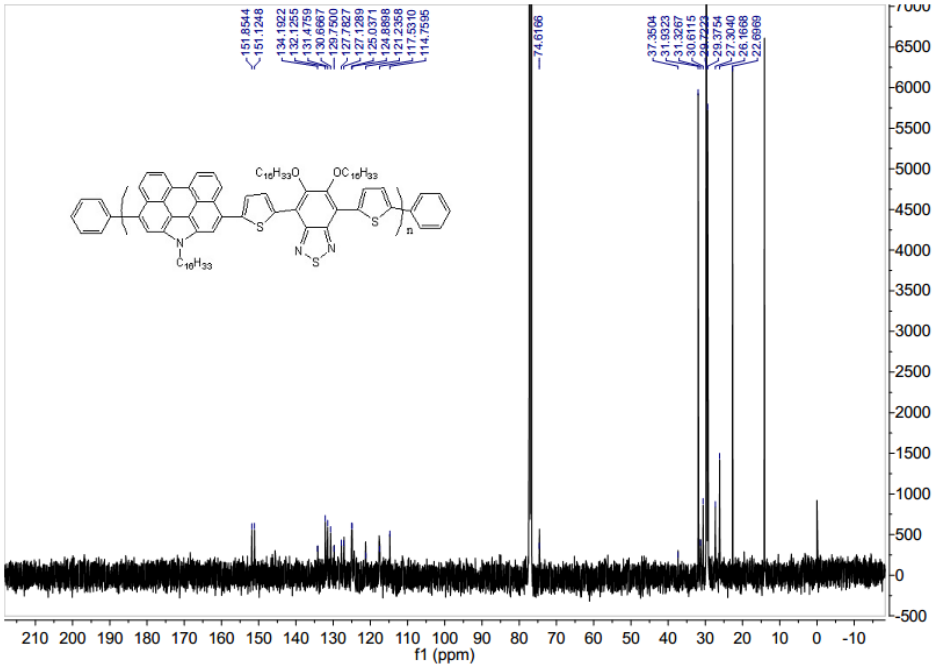

Figure S13. The ^{13}C NMR spectra of HXS-3.

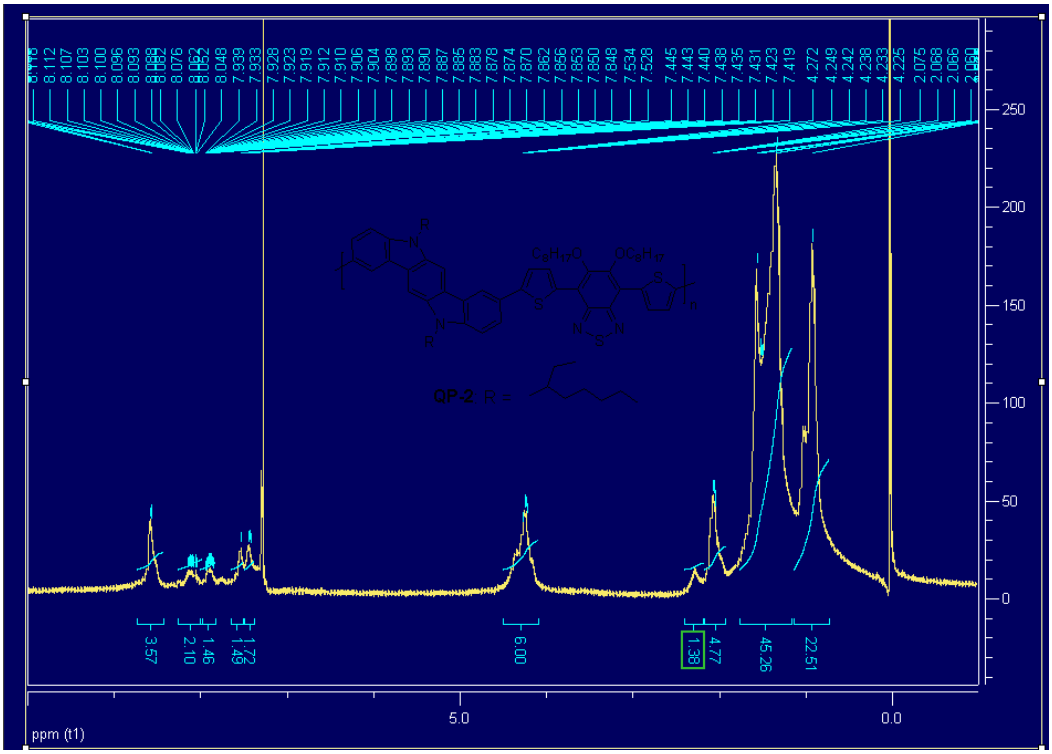

Figure S14. The ^{1}H NMR spectra of HXS-4.

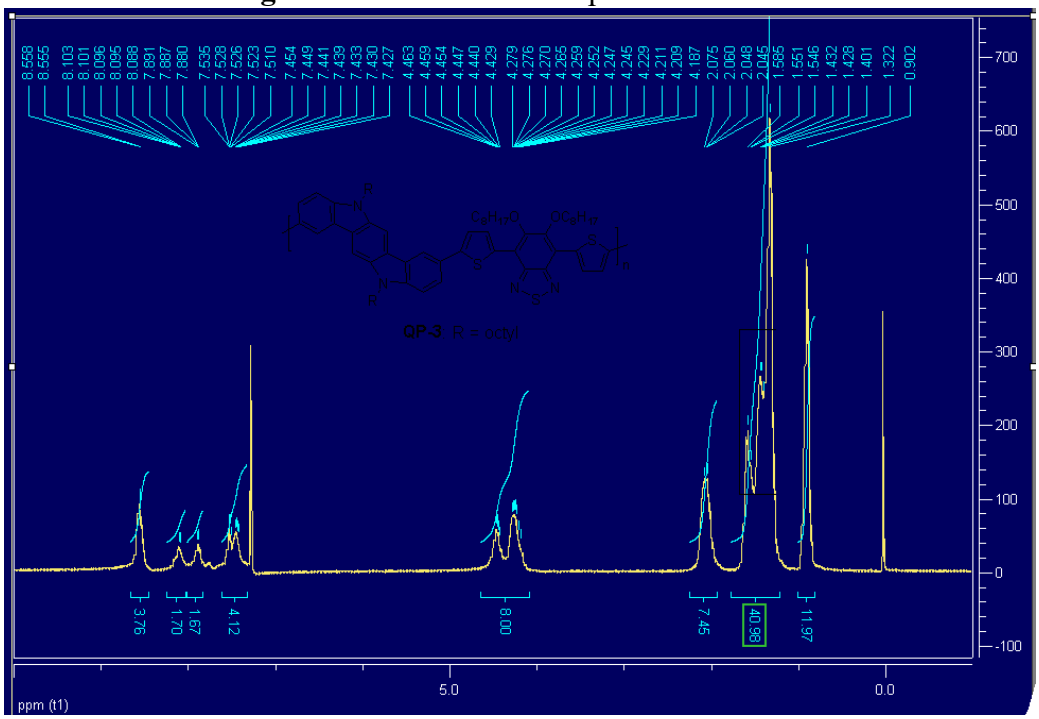

Figure S15. The ^{1}H NMR spectra of HXS-5.

[1] Qin, R.-P.; Song, G.-L.; Jiang, Y.-R.; Bo, Z.-S. Chem. J. Chin. Univer. **2012,** *33* (4), 828-832.

[2] Qin, R.; Li, W.; Li, C.; Du, C.; Veit, C.; Schleiermacher, H.-F.; Andersson, M.;

Bo, Z.; Liu, Z.; Inganäs, O.; Wuerfel, U.; Zhang, F., J. Am. Chem. Soc. **2009,** *131* (41), 14612-14613.
[3] Zeng, Z.; Ishida, M.; Zafra, J. L.; Zhu, X.; Sung, Y. M.; Bao, N.; Webster, R. D.; Lee, B. S.; Li, R.-W.; Zeng, W.; Li, Y.; Chi, C.; Lopez Navarrete, J. T.; Ding, J.; Casado, J.; Kim, D.; Wu, J. J. Am. Chem. Soc. **2013**, 135, 6363.
[4] L. Zhu, C. Jiao, D. Xia, J. Wu. Tetrahedron Letters 52 (**2011**) 6411–6414.
[5] Z. Zeng, S. Lee, M. Son, K. Fukuda, P. M. Burrezo, X. Zhu, Q. Qi, R. Li, J. T. L. Navarrete, J. Ding, J. Casado, M. Nakano, D. Kim, and J. Wu. J. Am. Chem. Soc. **2015**, 137, 8572.
[6] R. Qin, Z. Bo, Macromol. Rapid Commun., 33, 87 (**2012**).